A Back Propagation Network based MPPT Algorithm for Grid-Tied Wind Energy System with Vienna Rectifier

Damodhar Reddy*, Sudha Ramasamy**‡

*School of Electrical Engineering, Vellore Institute Technology, Vellore, 632014.

**Division of Production Systems, Innovatum, University West, Trollhattan, Sweden.

(damodhar_reddy@ymail.com, sudha.ramasamy@hv.se)

‡ Corresponding Author; Dr. Sudha Ramasamy, Division of Production Systems, Innovatum, University West, Trollhattan, Sweden.

sudha.ramasamy@hv.se.

Received: 02.04.2019 Accepted:20.05.2019

Abstract- This paper presents a boost type Vienna Rectifier with a back propagation network algorithm for maximum power point tracking (MPPT) from the wind energy system. The preferred control algorithm deals with non-linear problems with improved conversance precision and reduced learning time. In this system, boost type Vienna Rectifier is employed as a machine side converter for single stage energy conversion of AC to DC with the enhanced output voltage and a grid side converter worked for DC to AC conversion. Vienna Rectifier facilitates power flow with high power density, continuous sinusoidal input current, improved power factor and offers low voltage stress across the switches. The proposed system is designed to meet the load power demand of 1kW Active power with the combined contribution of the wind and the main grid. The resulting analysis of the Vienna Rectifier with the aforementioned control algorithm is validated through Matlab-Simulink for variable wind speeds.

Keywords-Wind energy system, Elman back propagation neural network, permanent magnet synchronous generator (PMSG), Vienna Rectifier, grid side converter.

1. Introduction

The small and medium scale wind energy conversions allow extraction of wind energy where there is no possibility to install the large wind turbine systems. Islanded or grid-connected wind energy systems are getting more attraction towards clean energy production. Due to rapid advancement in the aerodynamic design of small size wind turbines, power converters and MPPT algorithms can enhance the extraction of wind energy. Moreover, developments in the design of variable- wind speed turbine generators [1] can increase the effective conversion of energy from the variable wind speeds over fixed-speed turbine systems. In contrast to the other possible wind turbine generators, the PMSGs are more appropriate for variable wind turbine speeds [2, 3] which can allow direct coupling to the turbine with the absence of gear-box. In addition to that, the PMSGs provide higher efficiency with reducing flickers, low mechanical stress and minimized copper losses [4, 5]. Since the PMSG is an AC machine, AC to DC power electronic converters are required to feed the DC loads or DC-bus and AC/DC/AC-AC/AC are required to feed the AC loads or grid as well [6]. There are possible two-level and three level converter configurations available to supply the demand in single or two-stage conversion [7, 8].

Generally, two-level converters are widely used in the renewable energy conversion systems for AC to DC, DC to DC and DC to AC conversion [9, 10] but this kind of converters is limited to low power and low-frequency operation. In order to meet the high power and high-

frequency applications [11], a single stage three-level/three-switch Vienna Rectifier is introduced in this paper which acts as a machine side converter (MSC) with high power density for the Wind energy system to feed the DC-bus [12]. The design of Vienna Rectifier is proposed by J. W. Kollar in 1993 for three-phase systems to convert AC to DC with enhancing voltage and improved power factor [13]. The proposed rectifier provides high efficiency, high power density and reduced switching losses in AC to DC conversion systems [14, 15]. In recent years, Vienna Rectifier is engaged in the applications of a telecommunication system, data centers, shipboards, etc and now extended to the Wind energy systems for AC to DC conversion. In case of grid-connected wind energy system configuration, PWM (pulse width modulation) controller [16, 17] base voltage source inverters or current source inverters [18, 19] employed as grid side converters in order to regulate DC bus voltage and as well as to control the active and reactive power components [20, 21].

In order to obtain optimum power point, researchers have proposed various MPPT control methods of indirect power control (IPC) methods [22] such as the tip-speed ratio (TSR) control which rely on the wind speed measurement, power signal feedback (PSF) and optimal torque controls (OTC) which rely on the wind turbine power curve. Also, various MPPT control methods of direct power control (DPC) methods have proposed in the literature such as perturbation & observation (P & O) [23, 24] method based on hill climb search algorithm (HCS) [25] which rely on turbine power curve without any previous knowledge. But the aforementioned algorithms have difficulties in estimating both the wind velocity and turbine speeds in real-time systems and plotting the power curve without any prior knowledge would extend the complexity of the system. In order to overcome the Pitfalls in the MPPT algorithms, intelligent control methods are introduced by the researchers such as fuzzy logic control (FLC) [26, 27], adaptive neuro-fuzzy systems (ANFIS) [28] and artificial neural network (ANN) based control algorithms, etc. In ANN, there are some popularly used MPPT control algorithms for renewable energy conversion systems are namely feedforward networks (FFNs), backpropagation neural networks (BPNNs) [29], Elman back propagation neural networks (EBPNNs) [30], generalized regression neural networks (GRNNs) [31] and radial basis function networks (RBFNs) [32, 33] etc. Here, feedforward networks and backpropagation neural networks algorithm have the limitations to deal with the higher order non-linear systems which result in low conversance precision and high learning time. An improved Elman back propagation neural network MPPT algorithm based grid-connected wind energy system is designed in this paper with boost type Vienna Rectifier. The Elman backpropagation algorithm is proposed by Elman in 1990, it is a partial recurrent network model widely used in dynamic identification systems [34]. It is a superior network than the feed-forward networks which results in high conversance precision and low learning rate in extracting the maximum power point in the wind turbine system. The modification has made to an improved Elman backpropagation network in order to get better precision values.

2. Model Description

The grid-connected wind energy system (WES) consists of the wind turbine (WT) coupled with the PMSG at which the wind energy is converted into a variable voltage and fed to a three-level/three switch Vienna Rectifier in the front-end for AC to DC conversion as shown in Fig.1. In this system, a pitch angle controller is engaged to control the output power mechanically. The output torque of the wind turbine is used to control the angular speed thus controlling the mechanical output power. The wind turbines are integrated with pitch angle so as to protect the wind generator for sudden wind gust due to higher wind speed. During lower wind speed the pitch of the blade is adjusted to rotate the rotor at higher speed thus increasing the power of the machine. During higher wind speed the pitch angle controller limits the speed of rotor thus protecting the generator and if the controller is not able to limit the rotor speed below the optimal speed it acts as a braking system. The pitch angle control and the rotational speed control are developed according to the variation in wind speed. An artificial neural network based Elman back propagation MPPT control algorithm is introduced in this system, in order to trace the maximum power point from the variable speed turbine. EBPNN based MPPT control algorithm is used to generate an optimal rotor speed (ω_{m_opt}) to get the maximum power (P_{max}) for the proposed system configuration at variable wind speeds. An ANN-based control algorithm is adapted for optimal power point extraction with reference to the optimal wind turbine speed. In the machine side converter (MSC), a vector control strategy is adopted with double closed loop regulation. The error signal estimated from the reference wind turbine speed and optimal wind turbine speed and it is given to the PI (proportional-integral) controller where the reference q-axis current (i^*_{sq}) is generated for the front-end control unit. Also, V_{sq} is generated from reference q-axis current. In order to reduce the copper loss, the *d-axis* component is set to zero and $\Delta V_{sq,}$ $\Delta V_{sd,}$ are added to the control strategy in order to enhance the dynamic response. Hence the switching signals are generated form PWM controller and delivered to the switches of the rectifier.

In the back-end converter controller, a direct power control (DPC) method is applied to regulate the DC-link voltage and to control the active (P_g) and reactive power (Q_g) and

compared with the reference components. In this, the P^*_g and Q^*_g are the rated values of the active and reactive components. Where the P^*_g is used to maintain the constant output voltage and whereas Q^*_g is determined by the power factor. The error signal is fed to the PI-controller and then PWM for control of the grid side converter. A vector control method is used to regulate the grid side parameters with double closed loop strategy in which the PI controllers are employed to regulate the *d-axis and q-axis* components. A grid side converter (GSC) (DC to AC) is connected to transform energy from machine side converter to the grid with the fixed voltage and frequency. The grid side converter controller is controlled by utilizing the grid voltages/currents and DC-link voltage. Here *d-axis and q-axis* current components are i_{gd} and i_{gq}. Similarly, the grid side voltage components of *d-axis and q-axis* are V_{gd} *and* V_{gq}.

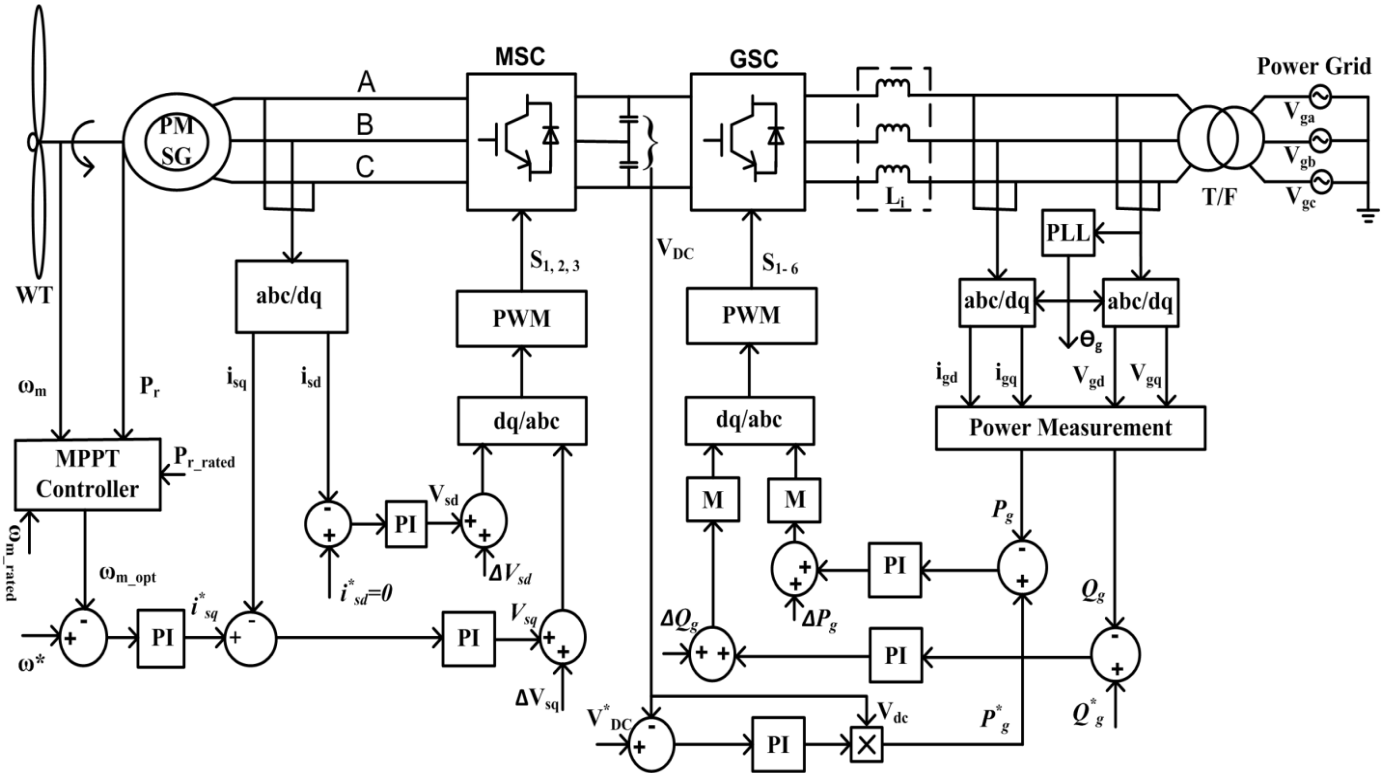

Fig.1 Circuit diagram of On-Grid Wind energy system

2.1 Wind Turbine Characteristics

The wind turbine power and speed characteristics are obtained as depicted in Fig.2 for different wind velocities. The wind turbine dynamic behavior relies on the power/torque coefficient and the output of the turbine is estimated by the wind velocity. The optimum output value of a wind turbine depends on the Tip speed ratio (λ) and pitch angle (β). The wind turbine mechanical torque (T_m) is written in terms of Sweep area of the turbine blades (A), Air density (kg/m^3), Pitch angle, power coefficient, wind velocity, and Tip speed ratio, which can be written as,

$$T_m = \frac{1}{2}\rho A C_p(\lambda,\beta)v^3 \frac{1}{\omega_m} \qquad (1)$$

Where, λ = Tip-ratio, ρ =Air density (kg/m3), β = Pitch angle (deg), C_p =Power Coefficient, A= Sweep area of turbine blades (m^2), ν = Wind speed (m/s) and ω_m = turbine angular velocity (rad/sec). The λ can be written as,

$$\lambda = \frac{\omega_m R}{v} \qquad (2)$$

Where R= turbine blade radius (m)

The turbine mechanical output power transferred to the PMSG is written as,

$$P_m = \frac{1}{2}\rho A C_p(\lambda,\beta)v^3 \qquad (3)$$

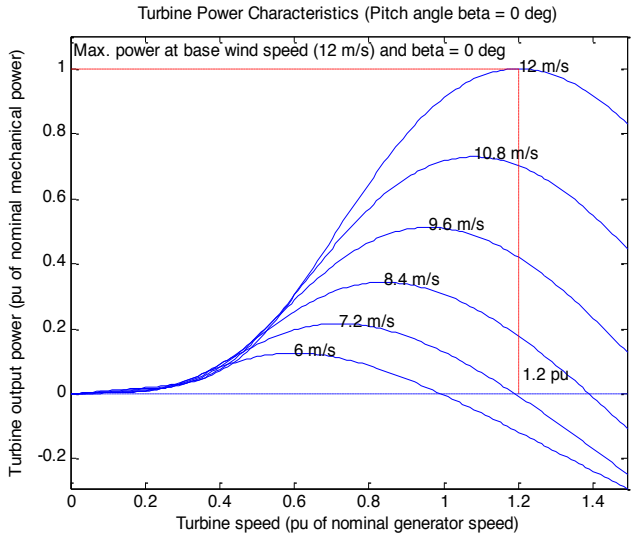

Fig.2 Speed and power characteristics

As shown in Fig.3, the regions of minimum and maximum power generation are represented between the cut-in and cut-out speed of the turbine. The pitch angle (β) control will be enabled for the wind speeds of below and above the base speed such as during lower wind speeds (between cut-in speed and rated speed) the pitch of the blade is adjusted to rotate the rotor at higher speed thus increasing the power of the machine. Similarly, during higher wind speeds (between rated speed and cut-out speed) the pitch angle controller limits the speed of the rotor thus protecting the generator.

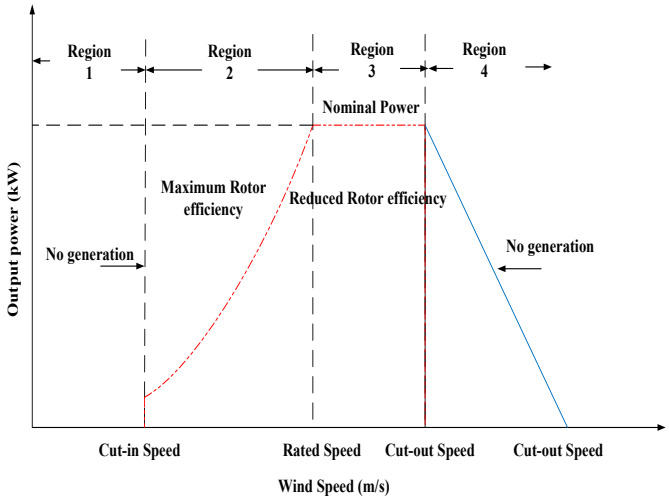

Fig.3 Output power and speed characteristics

2.2 Permanent Magnet Synchronous Generator

Since the rotor of the PMSG is associated with the turbine shaft, the mechanical power transferred to it and transformed into electrical energy (power). It can offer high power density, low rotor inertia, low copper loss with the absence of field winding. The dynamic model behavior of the PMSG is expressed in a *dq*-reference frame (Park transformation) to obtain accurate results during transients. The voltage equations are written in the rotor reference frame as follows,

$$V_{gq} = (R_g + pL_q)i_q + \omega_e(L_d i_d + \psi_f) \quad (4)$$

$$V_{gd} = (R_g + pL_d)i_d - \omega_e L_q i_d \quad (5)$$

Where, i_d, $V_{gd,}$ and i_q, V_{gq} are the *d-q* axis stator current and voltage respectively. L_d and L_q are the *d-q* axis inductance of generator, R_g refers to the stator winding resistance of the generator (Ω), ψ_f = Magnetic flux (wb) and ω_e is the speed of the generator. Where ω_e can be given as,

$$\omega_e = p_n \omega_m \quad (6)$$

The electromagnetic torque (T_e) of the generator is written as,

$$T_e = \frac{3}{2}[\psi_f i_q - (L_d - L_q)i_d i_q] \quad (7)$$

Hence, the dynamic model equation of the wind turbine is expressed as,

$$J\frac{d\omega_m}{dt} = T_e - T_m - F\omega_m \quad (8)$$

Where J= moment of inertia and F= Viscous friction coefficient. The design parameters chosen for the wind turbine and PMSG model are tabulated in Table. 1.

Table.1. Wind turbine and PMSG parameters

S. No	Wind system parameters	Ratings
1	Wind base speed	12m/s
2	Torque constant	1.8
3	Flux linkage	1.2Wb-t
4	Stator phase resistance	3.07Ω
5	Stator (armature) inductance	6.57mH
6	The maximum voltage at base speed	230V
7	Maximum output power at base speed	1kW

2.3 Boost Type Vienna Rectifier

The Vienna Rectifier circuit consists of six diodes, three bi-directional switches, and the output DC-link capacitor C as depicted in Fig.4. The DC-link capacitor is split into two to allow the mid-point configuration of the circuit with equal voltage distribution as ($+\frac{V_{DC}}{2}$) at capacitor C_1 and ($-\frac{V_{DC}}{2}$) at capacitor C_2, hence the total output voltage (V_{DC}) at DC-link is the sum of the voltage across C_1 (V_{DC1}) and C_2 (V_{DC2}).

Due to the large DC-link capacitance at the output terminals, the voltage across capacitor C_1 and C_2 are constant for every periodic switching and the neutral point voltage is zero in the steady state.

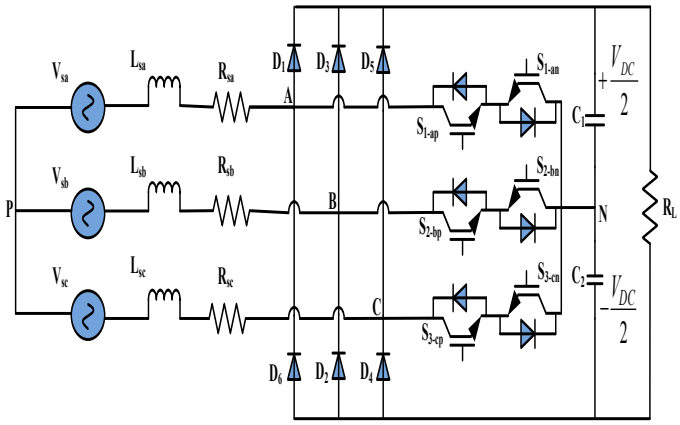

Fig.4 Circuit diagram of boost type Vienna Rectifier

The rectifier circuit operation is considered for single-phase approach in order to analyze the flow of current in each mode (Phase-A) as shown in Fig.4a to Fig.4d and the similar circuit operation is apples for the phase-B and phase-C. The modes of operation of the Vienna Rectifier for phase-A is as follows,

Mode.1: For S_1=0 (switch-OFF), $V_{sa} > 0$ and $i_a > 0$: the current flows from phase (P) to neutral (N) through the diode D_1, L_{sa}, and R_{sa} as depicted in Fig.5a where S_{1_ap}=1 and S_{1_an}=0. **For S_1=0, $i_a < 0$, $V_{sa} < 0$:** the current flows from neutral to phase through the diode D_6 as shown in Fig.4b where $S_{1\_an} = 1$ and $S_{1\_ap} = 0$.

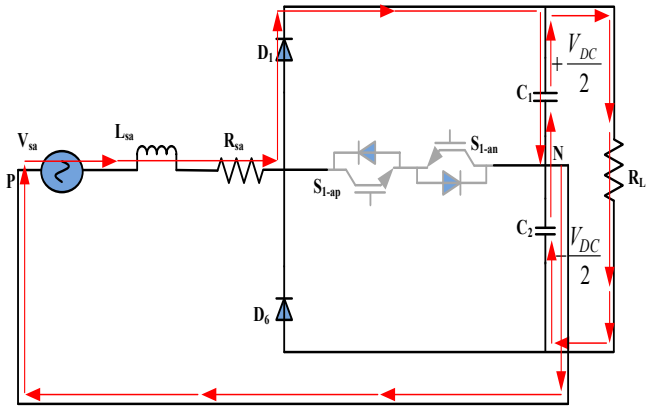

Fig.4a) $i_a > 0$, $V_{sa} > 0$, $S_{1\_ap} = 1$, $S_{1\_an} = 0$

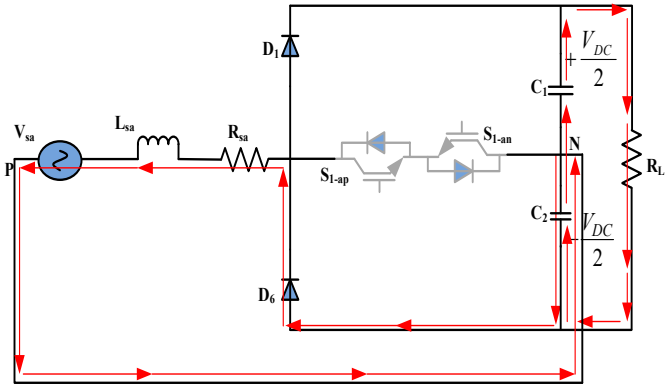

Fig.4b) $i_a < 0$, $V_{sa} < 0$, $S_{1\_ap} = 0$, $S_{1\_an} = 1$

Mode.2: For S_1=1 (switch-ON), $V_{sa} > 0$ and $i_a > 0$: the current flows from phase (P) to neutral (N) through L_{sa}, R_{sa} and the switch S_1 where S_{1_ap}=1 and S_{1_an}=0 as depicted in Fig.4c where S_{1_ap}=1 and S_{1_an}=0. **For S_1=1, $i_a < 0$, $V_{sa} < 0$:** the current flows from neutral to phase through the switch S_1 as shown in Fig.4d where $S_{1\_an} = 1$ and $S_{1\_ap} = 0$. The switching pattern is tabulated for three switches in Table.2 along with the corresponding voltages and currents with respect to a neutral point.

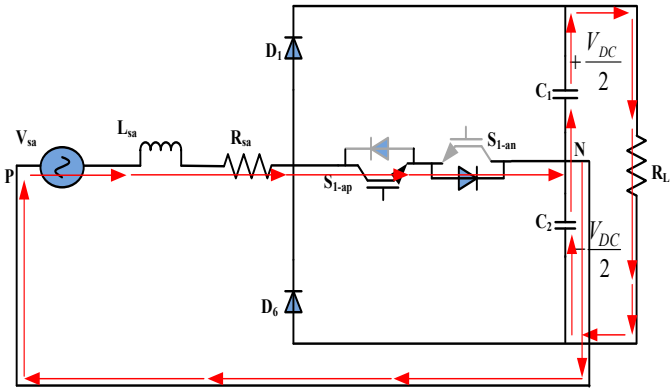

Fig.4c) $i_a > 0$, $V_{sa} => 0$, $S_{1\_ap} = 1$, $S_{1\_an} = 0$

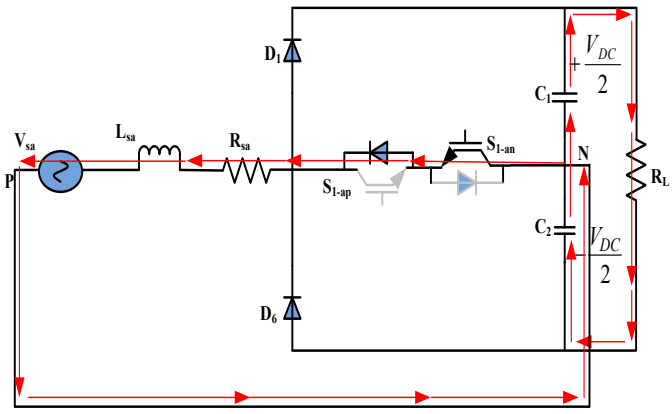

Fig.4d) $i_a < 0$, $V_{sa} < 0$, $S_{1\_ap} = 0$, $S_{1\_an} = 1$

Table.2. Switching states corresponding voltages and currents with respect to the neutral point

S_1	S_2	S_3	V_{AN}	V_{BN}	V_{CN}	i_N
0	0	0	$+\frac{V_{DC}}{2}$	$-\frac{V_{DC}}{2}$	$-\frac{V_{DC}}{2}$	0
0	0	1	$+\frac{V_{DC}}{2}$	$-\frac{V_{DC}}{2}$	0	$-i_c$
0	1	0	$+\frac{V_{DC}}{2}$	0	$-\frac{V_{DC}}{2}$	$-i_b$
0	1	1	$+\frac{V_{DC}}{2}$	0	0	i_a
1	0	0	0	$-\frac{V_{DC}}{2}$	$-\frac{V_{DC}}{2}$	$-i_a$
1	0	1	0	$-\frac{V_{DC}}{2}$	0	i_b
1	1	0	0	0	$-\frac{V_{DC}}{2}$	i_c
1	1	1	0	0	0	0

Three phase source voltages V_{sa},V_{sb} ,V_{sc} can be written as,

$$\left.\begin{aligned} V_{sa} &= E_m \sin(wt) \\ V_{sb} &= E_m \sin(wt - \frac{2\pi}{3}) \\ V_{sc} &= E_m \sin(wt + \frac{2\pi}{3}) \end{aligned}\right\} \quad (9)$$

The voltage equations with respect to the neutral point of the Vienna Rectifier are written as,

$$\left.\begin{aligned} V_{sa} &= i_{sa}R_{sa} + L\frac{di_{sa}}{dt} + V_{AN} \\ V_{sb} &= i_{sb}R_{sb} + L\frac{di_{sb}}{dt} + V_{AN} \\ V_{sc} &= i_{sc}R_{sc} + L\frac{di_{sc}}{dt} + V_{AN} \end{aligned}\right\} \quad (10)$$

Where L=source inductance, R= source resistance, and $V_{sa, sb, sc}$ = Vienna rectifier input terminal voltage which relies on the switching state and flow of current in the circuit. V_{AN}, V_{BN}, and V_{CN} are the switch voltages which can be expressed as the function of current and state of the switch.

$$\left.\begin{aligned} V_{AN} &= \frac{V_{DC}}{2}\text{sgn}(i_a)(1-S_1) \\ V_{BN} &= \frac{V_{DC}}{2}\text{sgn}(i_b)(1-S_2) \\ V_{CN} &= \frac{V_{DC}}{2}\text{sgn}(i_c)(1-S_3) \end{aligned}\right\} \quad (11)$$

Where V_{DC} is the DC – link capacitor voltage of the Vienna rectifier and 'sgn' is the signum function of $i_{a,b,c.}$ Here, V_{DC} can be written as,

$$\left.\begin{aligned} V_{DC} &= V_{DC1} + V_{DC2} \\ \Delta V &= V_{DC1} - V_{DC2} \end{aligned}\right\} \quad (12)$$

Where V_{DC1}= voltage across capacitor C_1 and

V_{DC2} = voltage across capacitor C_2.

The design parameters considered for the machine side converter at turbine base speed are tabulated in Table.3. The input and output voltage will vary as the wind turbine speed changes.

Table.3. Circuit parameters for base speed (12 m/s)

S. No	Circuit parameters	Ratings
1	Three phase input voltage ($V_{sa, sb, sc}$)	230V
2	Maximum Output Voltage	400V
3	The power rating for wind unit	1kW
4	Input inductance (L_i =$L_{sa, sb, sc}$)	10mH
5	Input resistance (R_i =$R_{sa, sb, sc}$)	0.01Ω
6	Input filter capacitance (C_f = $C_{sa, sb, sc}$)	100uF
7	DC-link capacitance ($C = C_1 + C_2$)	200 µF
8	Diode resistance (R_{ON})	0.001Ω
9	Load resistance (R)	160Ω
10	Maximum output power (P)	1kW

2.4 EBPNN Control Algorithm

Elman neural network is similar to the backpropagation network which consists of four layers called input layer (i), hidden layer (j), context layer (r) and an output layer (k) as depicted in Fig.5. In the context layer, the context neurons are employed as memory units to store the previous outputs of the hidden neurons. Due to low convergence precision and learning speed in conventional ENN (Elman neural network), the feedback signals are considered in the improved EBPNN (Elman Back Propagation Neural Network) to get the better learning efficiency. In addition to that, the neurons are made sensitive to the history of the input data, self-connection of context nodes and output feedback nodes are added. Improved EBPNN is having the capability of dealing with non-linear problems. Moreover, it can improve convergence precision and minimize learning time.

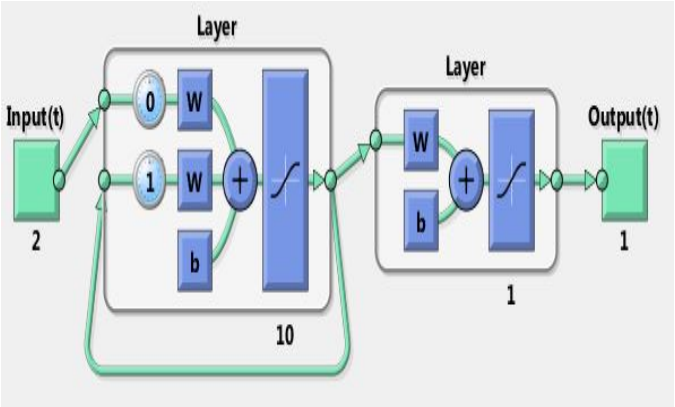

Fig.5 Representation improved EBPNN structure

The input variables to the EBPNN are $e_1^1 = \omega_r^* - \omega_r$ and $e_2^1 = P_r^* - P_r$, where the control signal is defined as i_q^*. The signal propagation and basic function in each layer are written as follows,

i) The input layer (i): In this layer, the node is written as,

$$x_i^1(n) = f_i^1(net_i^1(n)) = net_i^1 = e_i^1(n), \quad i=1, 2, 3,\ldots \tag{13}$$

Where '*n*' is the n[th] iteration, $e_i^1(n)$ is the input of the layer and $x_i^1(n)$ is the output of the layer.

ii) Hidden layer (j): In this layer, the node is written as,

$$x_j^2(n) = S(net_j^2(n)), \; j=1, 2, 3,\ldots \tag{14}$$

$$net_j^2(n) = \sum_i W_{ij} * x_i^1(n) + \sum_r W_{rj} * x_r^3(n),$$

$$r=1, 2, 3,\ldots \tag{15}$$

Where $x_i^1(n)$, $x_r^3(n)$ are the inputs to the hidden layer and $x_j^2(n)$ is the output of the hidden layer. And similarly, W_{ij} and W_{rj} are the connecting weights to the input neurons to the hidden layer and context layer and S(x) is the sigmoid function represented as $S(x) = \frac{1}{1+e^{-x}}$, where $x=net_j^2$.

iii) context layer (r): in this layer, the node output is written as,

$$x_r^3(n) = \alpha x_r^3(n-1) + x_j^2(n-1) \tag{16}$$

Where 'α' is a self-connecting feedback gain.

iv) Output layer (k): In this layer, the node output is written as,

$$y_k^4(n) = f_k^4(net_k^4(n)) = net_k^4(n) = i_q^*,$$

$$k=1, 2, 3,\ldots \tag{17}$$

$$(net_k^4(n) = \sum_j W_{jk} + x_j^2(n) \tag{18}$$

After initialization of the EBPNN, a supervised learning method is used to train the data based on the gradient descent which minimizes the error function. It employs as to regulate the parameters of the EBPNN through the training patterns. By recursive application of the chain rule, the error function of each layer is estimated and weights are added. In this proposed system configuration, the optimal wind data is considered and the corresponding optimal data values of speed and power are estimated to train the system for maximum power extraction. The resultant of the controller is fed to the PI controller where vector control strategy is employed for dynamic system response.

2.5 Grid Side Converter

The aim of the grid side converter is to transfer the energy from a front-end conversion unit to the main grid and the load. Therefore, GSC acts as an AC to DC conversion unit at the back-end of the system in order to regulate the DC-link voltage and it can control the active and reactive power of the system. A direct power control method is considered in this system to control the instantaneous values of the active and reactive power components which are decoupled into synchronous *d-q* reference frame. Here two control loops are

enabled: the inner current loop is used for active and reactive power control and outer loop is engaged for DC-link voltage control. If the grid voltage space vector is oriented on *d-axis* then V_{gd} = V and V_{gq} = 0. Where V_{gd} and V_{gq} are the grid voltage components of *d-axis* and *q-axis* respectively. The voltage balance equations are written based on the rotating reference frame as follows,

$$L_i \frac{di_{gd}}{dt} = E_{id} - R_i i_{gd} + \omega L_i i_{gq} - V \quad (19)$$

$$L_i \frac{di_{gq}}{dt} = E_{iq} - R_i i_{gq} - \omega L_i i_{gd} \quad (20)$$

Where i_{gd} and i_{gq} are the current components of *d-axis* and *q-axis* respectively.

Similarly, E_{id} and E_{iq} are the inverter voltage components of *d-axis* and *q-axis* respectively. R_i = line resistance and L_i = line resistance. Therefore, active power (P) and reactive power (Q) are written in terms of grid voltage and line current components as follows,

$$P = \frac{3}{2} v_{gd} i_{gd} \quad (21)$$

$$Q = \frac{3}{2} v_{gd} i_{gq} \quad (22)$$

3. Result and Discussion

The grid-connected wind energy system is designed based on Elman back propagation network algorithm with boost type Vienna Rectifier. In this system, the wind velocity is considered between 9 m/s to 16 m/s as a variable input to the wind turbine, which results in variable turbine mechanical power output and PMSG output power.

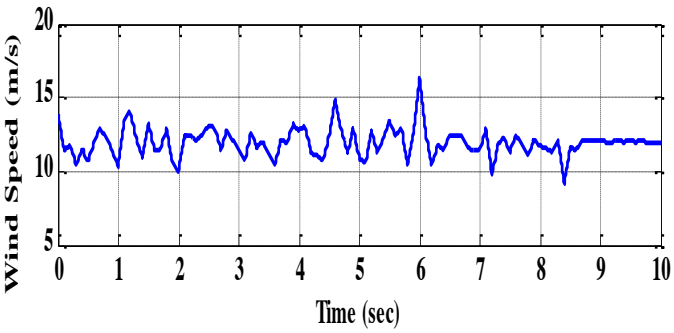

Fig.6 wind velocity

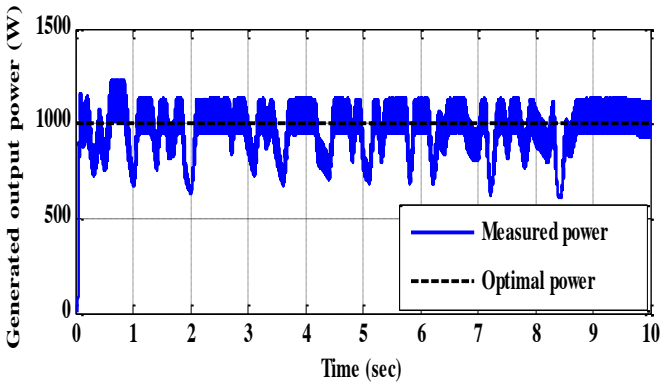

Fig.7 Power output of the PMSG

From Fig.7 as displayed, it is observed that the output voltage of PMSG is varied as the wind turbine speed changes. For the above base speeds of wind the pitch angle control is enabled to control rotor speed and as well as the power output of the PMSG.

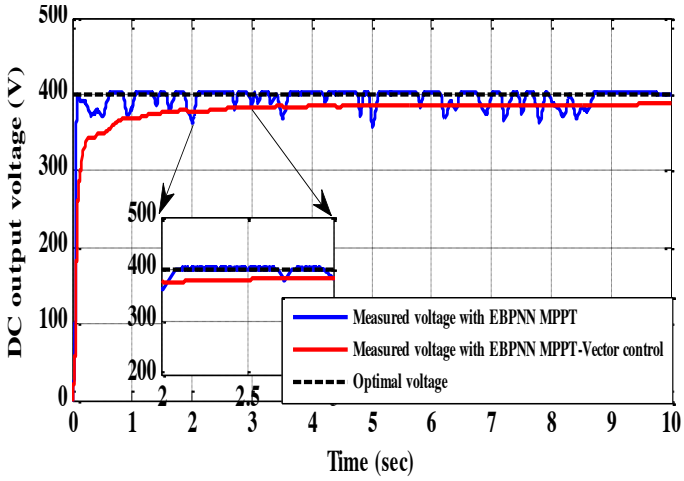

Fig.8 Vienna Rectifier DC output voltage for off-grid WES

The enhanced output voltage of Vienna Rectifier is recorded as displayed in Fig.8 with respect to the input parameters. The DC output voltage and current are measured for both EBPNN and EBPNN with vector control for the optimal values as shown in Fig.8 and Fig.9 respectively. The corresponding output power of Vienna Rectifier is shown in Fig.10. The optimal values of output voltage, current, and power of the Vienna Rectifier are measured and tabulated in Table.4 based on the input parameters for variable wind turbine speeds.

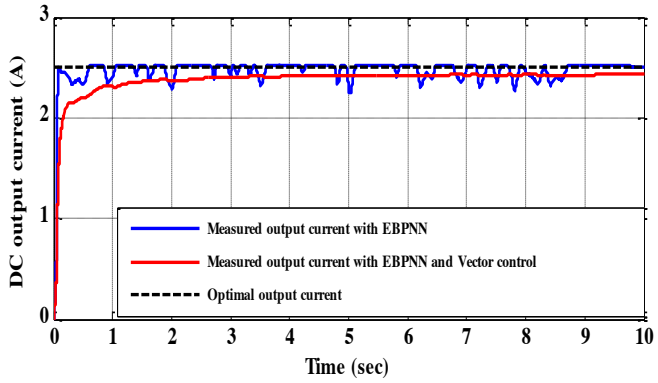

Fig.9 Vienna Rectifier DC output current for off-grid WES

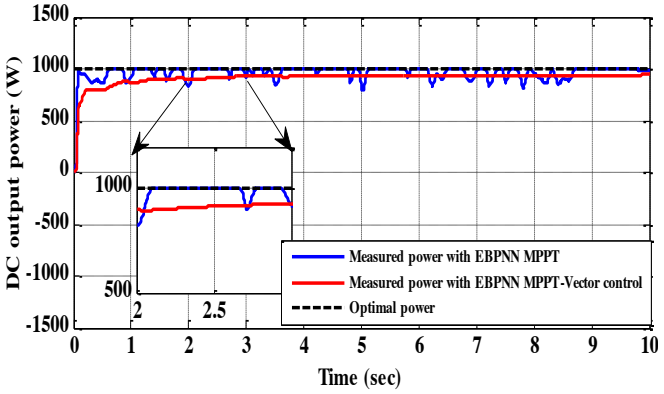

Fig.10 Vienna Rectifier DC output power for off-grid WES

Table.4. Vienna Rectifier output parameters for different wind speeds

Parameters	Output parameters of Vienna Rectifier	
Wind speed (m/s)	Below base speed	Above base speed
DC output voltage (V)	397.3V	400V
DC output current (A)	2.5A	2.5A
DC output power (W)	984W	1000W

It is obtained that the voltage of the inverter, load, and the grid is maintained at a constant value (peak voltage of 400) of 282.84V, 50Hz without any fluctuations even for large variations in the front-end conversion unit. The output waveforms of voltage and current of inverter load and grid are presented in Fig.11, Fig.12 and Fig.13 respectively.

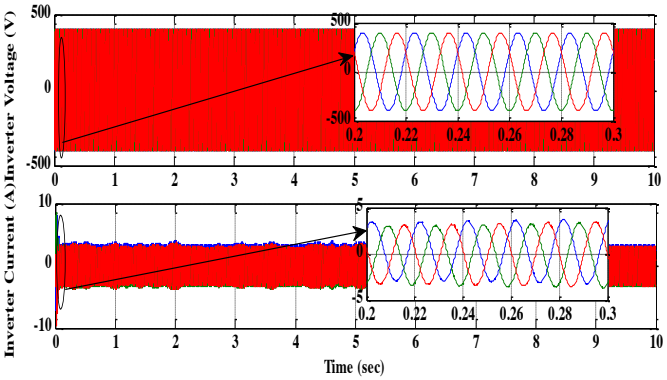

Fig.11 Inverter voltage and current

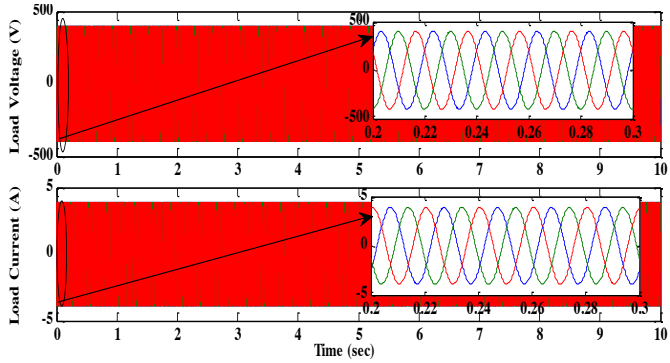

Fig.12 Load voltage and current

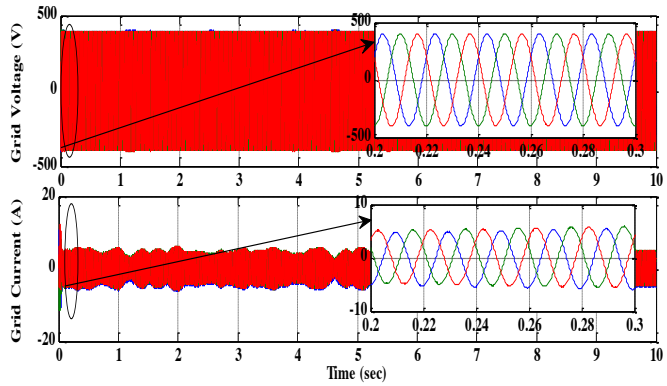

Fig.13 Grid voltage and current

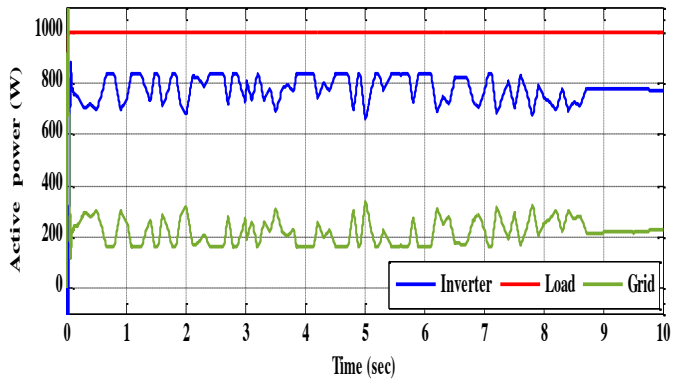

Fig.14 Active power of load, inverter, and grid

The power demand of a load of 1kW active power is supplied by the grid side converter and grid. The active power of inverter, load and grid are shown in Fig.14 for variable wind speeds. The contribution of active power from the wind energy system and the grid is recorded for comparative analysis and tabulated in Table.5 at below base speed and above base speed.

Table.5. Load, inverter, and grid output parameters for different wind speeds

Parameters	Average Active Power (W) =1000	
Wind speed (m/s)	Below base speed	Above base speed
Inverter output	756.4	830.2
Grid output	242.2	168.5
Load output	998.7	998.7

4. Conclusion

The grid-connected wind energy system is presented with boost type Vienna Rectifier at the front-end and a PWM converter (GSC) is at the back-end of the proposed system configuration. An Elman back propagation neural network based MPPT is adopted for maximum power point tracking with fast conversance precision and reduced learning time. At wind turbine base speed of 12 m/s, a 230V AC is generated form PMSG is converted into 400V DC and fed to grid side converter for DC to AC conversion. The output power of GSC is delivered to the load and the grid at different power level form the GSC. The load demand of 1kW active power is supplied by the GSC and grid with a combined contribution of 830.2W and 168.5W in order to maintain a continuous supply. Hence the proposed system configuration is very significant in the renewable energy conversion systems and the efficient energy conversion is possible by the boost type Vienna Rectifier with an artificial neural network based MPPT control algorithms. This kind of Wind energy system is more suitable for the off-grid and grid-tied mode of operation to feed the load demand in rural and urban areas.

References

[1] Ayaz M, Colak I, Bayindir R. Matlab/gui based wind turbine generator types on smart grid systems. In2016 IEEE International Conference on Renewable Energy Research and Applications (ICRERA) 2016 Nov 20 (pp. 1158-1162). IEEE.

[2] Xie D, Lu Y, Sun J, Gu C. Small signal stability analysis for different types of PMSGs connected to the grid. Renewable Energy. 2017 Jun 1;106:149-64.

[3] Mokhtari Y, Rekioua D. High performance of Maximum Power Point Tracking Using Ant Colony algorithm in wind turbine. Renewable Energy. 2018 Oct 1;126:1055-63.

[4] Yasa Y, Mese E. Design and analysis of generator and converters for outer rotor direct drive gearless small-scale wind turbines. In2014 International Conference on Renewable Energy Research and Application (ICRERA) 2014 Oct 19 (pp. 689-694). IEEE.

[5] Soufi Y, Kahla S, Sedraoui M, Bechouat M. Optimal control based RST controller for maximum power point tracking of wind energy conversion system. In2016 IEEE International Conference on Renewable Energy Research and Applications (ICRERA) 2016 Nov 20 (pp. 1168-1172). IEEE.

[6] Xia Y, Ahmed KH, Williams BW. A new maximum power point tracking technique for permanent magnet synchronous generator based wind energy conversion system. IEEE Transactions on Power Electronics. 2011 Dec;26(12):3609-20.

[7] de Freitas TR, Menegáz PJ, Simonetti DS. Rectifier topologies for permanent magnet synchronous generator on wind energy conversion systems: A review. Renewable and Sustainable Energy Reviews. 2016 Feb 1;54:1334-44.

[8] Kalpana R, Singh B, Bhuvaneswari G. Design and Implementation of Sensorless Voltage Control of Front-End Rectifier for Power Quality Improvement in Telecom System. IEEE Transactions on Industry Applications. 2018 May;54(3):2438-48.

[9] Lee CY, Chen PH, Shen YX. Maximum power point tracking (MPPT) system of small wind power generator using RBFNN approach. Expert Systems with Applications. 2011 Sep 15;38(10):12058-65.

[10] Reddy D, Ramasamy S. Single Stage Energy Conversion through RBFN Controller based Boost Type Vienna Rectifier for Wind Turbine System. GAZI UNIVERSITY JOURNAL OF SCIENCE. 2017 Jan 1;30(4):253-66.

[11] Ajami A, Alizadeh R, Elmi M. Design and control of a grid tied 6-switch converter for two independent low power wind energy resources based on PMSGs with MPPT capability. Renewable Energy. 2016 Mar 1;87:532-43.

[12] Dang C, Tong X, Yin J, Huang J, Xu Y. The neutral point-potential and current model predictive control method for Vienna rectifier. Journal of the Franklin Institute. 2017 Nov 1;354(17):7605-23.

[13] Kolar JW, Friedli T. The essence of three-phase PFC rectifier systems—Part I. IEEE Transactions on Power Electronics. 2013 Jan;28(1):176-98.

[14] Lai R, Wang F, Burgos R, Boroyevich D, Jiang D, Zhang D. Average modeling and control design for VIENNA-type rectifiers considering the DC-link voltage balance. IEEE Transactions on Power Electronics. 2009 Nov;24(11):2509-22.

[15] RAMASAMY S, Reddy D. Design of a Three-phase Boost Type Vienna Rectifier for 1kW Wind Energy Conversion System. International Journal of Renewable Energy Research (IJRER), 30;7(4):1909-18, Dec 2017.

[16] Boulouiha HM, Allali A, Laouer M, Tahri A, Denai M, Draou A. Direct torque control of multilevel SVPWM inverter in variable speed SCIG-based wind energy conversion system. Renewable Energy. 2015 Aug 1;80:140-52.

[17] Quraan M, Farhat Q, Bornat M. A new control scheme of back-to-back converter for wind energy technology. In2017 IEEE 6th International Conference on Renewable Energy Research and Applications (ICRERA) 2017 Nov 5 (pp. 354-358). IEEE.

[18] Thongam JS, Bouchard P, Beguenane R, Fofana I. Neural network based wind speed sensorless MPPT controller for variable speed wind energy conversion systems. InElectric Power and Energy Conference (EPEC), 2010 IEEE 2010 Aug 25 (pp. 1-6). IEEE.

[19] Zhao H, Zheng TQ, Li Y, Du J, Shi P. Control and Analysis of Vienna Rectifier Used as the Generator-Side Converter of PMSG-based Wind Power Generation Systems. Journal of Power Electronics. 2017 Jan;17(1):212-21.

[20] Xu G, Liu F, Hu J, Bi T. Coordination of wind turbines and synchronous generators for system frequency control. Renewable Energy. 2018 Jun 1.

[21] Errami Y, Ouassaid M, Maaroufi M. Optimal power control strategy of maximizing wind energy tracking and different operating conditions for permanent magnet synchronous generator wind farm. Energy Procedia. 2015 Aug 1;74:477-90.

[22] Chen J, Jiang L, Yao W, Wu QH. A feedback linearization control strategy for maximum power point tracking of a PMSG based wind turbine. In2013 International Conference on Renewable Energy Research and Applications (ICRERA) 2013 Oct 20 (pp. 79-84). IEEE.

[23] Heydari M, Smedley K. Comparison of maximum power point tracking methods for medium to high power wind energy systems. InElectrical Power Distribution Networks Conference (EPDC), 2015 20th Conference on 2015 Apr 28 (pp. 184-189). IEEE.

[24] D. Reddy and S. Ramasamy, "A fuzzy logic MPPT controller based three phase grid-tied solar PV system with improved CPI voltage," *2017 Innovations in Power and Advanced Computing Technologies (i-PACT)*, Vellore, 2017, pp. 1-6.

[25] Kumar D, Chatterjee K. A review of conventional and advanced MPPT algorithms for wind energy systems. Renewable and sustainable energy reviews. 2016 Mar 1;55:957-70.

[26] Aissa O, Moulahoum S, Babes B, Kabache N. Design and real time implementation of three-phase three switches three levels Vienna rectifier based on intelligent controllers. Applied Soft Computing. 2017 Jul 31;56:158-72.

[27] Ramasamy S, Reddy D, Saravanan S. Comparative Analysis of RBFN and Fuzzy-SVPWM Controller Based Boost Type Vienna Rectifier for 1kW Wind Energy Conversion System. Journal of Green Engineering. 2018 Apr 30;8(2):177-200.

[28] Meharrar A, Tioursi M, Hatti M, Stambouli AB. A variable speed wind generator maximum power tracking based on adaptative neuro-fuzzy inference system. Expert Systems with Applications. 2011 Jun 1;38(6):7659-64.

[29] Pathak G, Singh B, Panigrahi BK. Back-Propagation Algorithm-Based Controller for Autonomous Wind–DG Microgrid. IEEE Transactions on Industry Applications. 2016 Sep;52(5):4408-15.

[30] Hong CM, Ou TC, Lu KH. Development of intelligent MPPT (maximum power point tracking) control for a grid-connected hybrid power generation system. Energy. 2013 Feb 1;50:270-9.

[31] Hong CM, Chen CH. Intelligent control of a grid-connected wind-photovoltaic hybrid power systems. International Journal of Electrical Power & Energy Systems. 2014 Feb 1;55:554-61.

[32] Reddy D, Ramasamy S. Design of RBFN Controller Based Boost Type Vienna Rectifier for Grid-Tied Wind Energy Conversion System. IEEE Access. 2018;6:3167-75.

[33] Hong CM, Chen CH, Tu CS. Maximum power point tracking-based control algorithm for PMSG wind generation system without mechanical sensors. Energy conversion and management. 2013 May 1;69:58-67.

[34] Lin WM, Hong CM. A new Elman neural network-based control algorithm for adjustable-pitch variable-speed wind-energy conversion systems. IEEE transactions on power electronics. 2011 Feb;26(2):473-81.